THE ASTROPHYSICAL JOURNAL, 526:344–356, 1999 November 20

DYNAMICS OF LINE-DRIVEN WINDS FROM DISKS IN CATACLYSMIC VARIABLES. I. SOLUTION TOPOLOGY AND WIND GEOMETRY

ACHIM FELDMEIER AND ISAAC SHLOSMAN
Department of Physics and Astronomy, University of Kentucky, Lexington, KY 40506-0055; achim@pa.uky.edu, shlosman@pa.uky.edu
Received 1999 February 9; accepted 1999 July 2

ABSTRACT

We analyze the dynamics of two-dimensional stationary, line-driven winds from accretion disks in cataclysmic variable stars. The driving force is that of line radiation pressure, in the formalism developed by Castor, Abbott, & Klein for O stars. Our main assumption is that wind helical streamlines lie on straight cones. We find that the Euler equation for the disk wind has two eigenvalues, the mass-loss rate and the flow-tilt angle with the disk. Both are calculated self-consistently. The wind is characterized by two distinct regions, an *outer* wind launched beyond four white dwarf radii from the rotation axis and an *inner* wind launched within this radius. The inner wind is very steep, up to 80° with the disk plane, while the outer wind has a typical tilt of 60°. In both cases, the wind cone dispersion is small because of a good alignment between the wind and the radiative flux vectors from the disk. We, therefore, provide an insight into the formation of the biconical geometry of disk winds as suggested by observations and kinematical modeling. The wind collimation angle appears to be robust and depends on the disk temperature stratification only. The flow critical points lie high above the disk for the inner wind but close to the disk photosphere for the outer wind. Comparison with existing kinematical and dynamical models is provided. Mass-loss rates from the disk as well as wind velocity laws are discussed in the second paper in this series.

Subject headings: accretion, accretion disks — novae, cataclysmic variables — stars: mass loss — stars: winds, outflows

1. INTRODUCTION

Accretion disks are ubiquitous in astrophysical systems ranging from newborn stars to compact objects, such as white dwarfs, neutron stars and black holes, both stellar and galactic. Because of their high temperatures and large surface areas, disks appear to be among the most luminous objects in the universe. Strong dissipative processes that accompany accretion around compact objects can release radiation energy in and above the disk, leading naturally to radiation-driven winds, similar to winds from hot stars. Observational signatures of such winds have been unambiguously detected in cataclysmic variables (CVs) (Heap et al. 1978; Krautter et al. 1981; Klare et al. 1982; Córdova & Mason 1982) and in active galactic nuclei (hereafter AGNs; Arav, Shlosman, & Weymann 1997, and references therein), but understanding them proved to be challenging. In this and the following paper (Feldmeier, Shlosman, & Vitello 1999, hereafter Paper II), we focus on different aspects of disk winds in CVs, such as their two-dimensional geometry, solution topology, mass-loss rates, and velocity profiles. AGN disk winds will be discussed elsewhere.

Theoretical understanding of winds from accretion disks is hampered by their intrinsically multidimensional character and by the richness of various physical processes supplementing the basic hydrodynamics of the flow. A number of different driving mechanisms for disk winds have been predicted and analyzed, from magnetic torques to X-ray disk irradiation (i.e., Compton-heated and thermally driven winds) to resonance line pressure (e.g., Blandford & Payne 1982; Begelman, McKee, & Shields 1983; Córdova & Mason 1985; Woods et al. 1996). Disks in nonmagnetic CVs with high accretion rates, $\gtrsim 10^{-9}\ M_\odot\ \mathrm{yr}^{-1}$, have an energy output that peaks in the (far-) ultraviolet, similarly to O, B, and WR stars. Their spectra exhibit features which bear similarity to those found in hot and massive stars and which are attributed to winds driven by radiation pressure in resonance and subordinate lines of abundant chemical elements, i.e., so-called line-driven winds (LDWs). Observational evidence in favor of LDWs from hot stars and disks includes but is not limited to the P Cygni line profiles of C IV, N V and Si IV, ionization levels, high terminal velocities and their correlation with the luminosity, and UV line behavior during continuum eclipse in CVs.

The pioneering work by Lucy & Solomon (1970), Castor (1974), and Castor, Abbott, & Klein (1975, hereafter CAK) showed that O star winds result from scattering of radiation in the resonance lines of abundant elements. The elegantly formulated theory of the LDWs from O stars by CAK, Cassinelli (1979), Abbott (1980, 1982), Pauldrach, Puls, & Kudritzki (1986), and others (for a textbook account, see Lamers & Cassinelli 1999) was successfully applied to individual objects. Further refinements of this theory by Owocki & Rybicki (1984, 1985) and Owocki, Castor, & Rybicki (1988) addressed the issue of stability of the flow.

First application of the LDWs to accretion disks emphasized the nonspherical ionizing continuum and driving force as well as a biconical geometry of the outflow (Shlosman, Vitello, & Shaviv 1985; Vitello & Shlosman 1988). Under a broad range of conditions, disk atmospheres in CVs and AGNs become dynamically unstable because the line opacity effectively brings them into a super-Eddington regime. Continuum photons absorbed by the UV resonance lines and reemitted isotropically contribute to the momentum transfer to the wind. This process can be described as a resonant scattering that conserves the number of photons throughout the wind and results in terminal wind velocities of the order of the escape speed at the base of the flow.

The dynamics and radiation field of disk LDWs employed by Shlosman et al. (1985) and by Vitello & Shlosman (1988) were oversimplified. Both were approximated

by a one-dimensional planar model allowing for divergence of the flow streamlines and geometrical dilution of the radiation field. Nineteen resonance lines in the range of 500–1600 Å were included in the calculation of the radiation force. It was noted that disk LDWs are more restrictive than stellar winds and that their development is strongly governed by the ionization structure in the wind.

Subsequently, a variety of two-dimensional kinematical models for disk winds in CVs, supplemented by a three-dimensional radiation transfer in the Sobolev approximation, were explored (Shlosman & Vitello 1993; Vitello & Shlosman 1993). Calculations using an alternative Monte Carlo radiation transfer method, albeit with frozen-in ionization, gave similar results (Knigge, Woods, & Drew 1995). Constrained by synthetic line profiles and by calculated effects of varying basic physical parameters, such as accretion and mass-loss rates, temperature of the boundary layer, rotation, and inclination angle, the available phase space for wind solutions was sharply reduced. Wind-resonant scattering regions exhibiting a strongly biconical character regardless of the assumed velocity and radiation fields were identified and mapped. This allowed us to match the observed line shapes from a number of CVs and to put forward a number of predictions, which were verified in high-resolution *HST* observations (Shlosman, Vitello, & Mauche 1996; Mauche et al. 1999). Most important, rotation was positively identified as the dominant factor shaping the UV line profiles in CVs, thus confirming that the disk and not the white dwarf is the wind source.

The above one-dimensional dynamical and two-dimensional kinematical modelings suffered from uniqueness problems that can be removed only by invoking the two-dimensional wind dynamics. Recent successful attempts by Proga, Stone, & Drew (1998; hereafter PSD) to model the two-dimensional time-dependent radiation hydrodynamics of disk LDWs was a major breakthrough in our understanding of this phenomenon. PSD basically confirmed that kinematical models of disk winds had sampled the correct parameter range and provided the scaling laws between different wind characteristics, e.g., between mass-loss rate and accretion luminosity, and delineated the phase space for possible time-dependent solutions. A number of empirical relationships were put forward which require a physical explanation.

In this paper, we focus on the two-dimensional geometry of a disk LDW in the presence of a realistic radiation field in CVs. We analyze solutions of the wind Euler equation, emphasizing differences in the solution topology with that of CAK stellar winds. In Paper II, we address issues related to the mass-loss rates and velocity laws of CV winds. The possible contribution to wind driving by magnetic stresses is ignored (e.g., Blandford & Payne 1982; Pudritz & Norman 1986; Emmering, Blandford, & Shlosman 1992), as are jetlike outflows seen in other disk systems (Livio 1997).

This paper is organized as follows. Section 2 reviews the relevant aspects of CAK theory for LDWs from O stars. Section 3 addresses the two-dimensional geometry of disk LDWs, as well as the radiation field above the CV disk. Section 4 deals with an analytic solution for vertical winds above an isothermal disk, and § 5 analyzes the solution topology and flow geometry for tilted winds above a disk with a realistic temperature stratification. Section 6 compares our results with other models and observations, and § 7 summarizes our basic conclusions.

2. CAK THEORY FOR O STARS

2.1. *The Stellar Line Force*

The CAK theory for LDWs from O stars forms the basis for our model of CV winds and is therefore briefly summarized here. CAK assume a line-distribution function per unit ν and κ, from UV to IR,

$$N(\nu, \kappa) = \frac{1}{\nu}\frac{1}{\kappa_0}\left(\frac{\kappa_0}{\kappa}\right)^{2-\alpha}, \tag{1}$$

where ν is the line frequency and κ (in cm^2 g^{-1}) is the mass absorption coefficient normalized to κ_0, which refers roughly to the strongest driving line in the flow (Owocki et al. 1988). For the power exponent, $0 < \alpha < 1$ holds, where the lower limit corresponds to purely optically thin lines and the (unrealistic) upper limit to purely optically thick lines. Puls, Springmann, & Lennon (1999) derive $\alpha = \frac{2}{3}$ from Kramers's formula applied to resonance lines of hydrogenic ions. Similar values of α are obtained from detailed non-LTE calculations for dense O-supergiant winds (Pauldrach 1987; Pauldrach et al. 1994). On the other hand, for low-density winds, e.g., from B stars near the main sequence, $\alpha = \frac{1}{2}$ may be more appropriate (Puls, Springmann, & Owocki 1998). Therefore, we shall consider both cases $\alpha = \frac{1}{2}$ and $\alpha = \frac{2}{3}$ to study the effect of α on the structure of disk winds.

Using equation (1), the CAK force from all lines can be written in a general way that is applicable for both geometries (e.g., Owocki & Puls 1996),

$$\boldsymbol{g}_L = \kappa_0\, v_{\rm th}\, \frac{\Gamma(\alpha)}{1-\alpha}\frac{1}{c^2}\int d\omega\, I_\gamma\, \hat{\gamma}\, \tau_\gamma^{-\alpha}, \tag{2}$$

by means of the Sobolev approximation (Sobolev 1957). $\Gamma(\alpha)$ is the complete gamma function, c is the speed of light, $d\omega$ is the solid angle centered on $\hat{\gamma}$, and I_γ is the frequency-integrated intensity in this direction. The line optical depth in direction $\hat{\gamma}$ is given by

$$\tau_\gamma = \frac{\kappa_0\ v_{\rm th}\ \rho}{\hat{\gamma}\cdot\nabla(\hat{\gamma}\cdot\mathbf{v})}, \tag{3}$$

with gas density ρ, and $\hat{\gamma}\cdot\nabla(\hat{\gamma}\cdot\mathbf{v})$ being the gradient along $\hat{\gamma}$ of the velocity component in direction $\hat{\gamma}$. Note that $\kappa_0\ v_{\rm th}$ is independent of the ion thermal speed $v_{\rm th}$ and so is the line force. Assuming spherical symmetry, and adopting the "radial streaming" approximation of CAK, i.e., $\tau_\gamma \equiv \tau_r$, equation (2) simplifies to

$$g_L = (\kappa_0\, v_{\rm th})^{1-\alpha}\, \frac{\Gamma(\alpha)}{1-\alpha}\frac{F}{c^2}\left(\frac{dv/dr}{\rho}\right)^{\alpha}, \tag{4}$$

with frequency-integrated, radial flux F.

2.2. *Stellar Euler Equation*

For an isothermal, spherically symmetric stellar wind, the stationary Euler equation in dimensionless form can be written as

$$\left(1-\frac{A^2}{W}\right)W' = -1 - \frac{4A^2}{U} + EW'^{\alpha}, \tag{5}$$

where, after CAK, we introduced a radial coordinate $U = -R_*/r$, with R_* being the stellar radius. The sound speed, A, and the flow speed, $V = W^{1/2}$, are normalized to the photospheric escape speed from the reduced stellar mass,

$M(1-\Gamma)$, where Γ is the Eddington factor. The normalized wind acceleration is given by $W' = dW/dU = r^2 v v'/GM(1-\Gamma)$, with v the flow speed and $v' = dv/dr$. Note (1) the different meaning of the prime in W' and v' and (2) that the gravitational acceleration is normalized to -1, whereas CAK normalize it to $-\frac{1}{2}$. The constant E in equation (5) is given by

$$E = \frac{\Gamma(\alpha)}{1-\alpha}\left[\frac{\kappa_0\, v_{\rm th}}{4\pi GM(1-\Gamma)}\right]^{1-\alpha}\frac{L/c^2}{\dot{M}^{\alpha}}\,, \tag{6}$$

where G is the gravitational constant, L is the stellar luminosity, and $\dot{M}$ is the mass-loss rate, $\dot{M} = 4\pi r^2 \rho v$. Global solutions to equation (5) exist only above a certain, critical $E_{\rm cr}$, called an eigenvalue of the problem, i.e., below a *maximum allowable* mass-loss rate. In the zero sound speed limit, $A = 0$, the differential equation (5) separates into an algebraic equation,

$$P \equiv W' + 1 - EW'^{\alpha} = 0\,, \tag{7}$$

and a trivial differential equation $W' = \text{const}$, which leads to the CAK velocity law, $v(r) = v_\infty(1 - R_*/r)^{1/2}$, where v_∞ is the flow terminal velocity. The Euler equation in the form given in equation (7) is particularly simple and its terms have a straightforward physical meaning, namely, inertia, gravity, and line force.

2.3. *The Stellar Wind Topology: Critical Point of the Flow*

We now consider solutions to equation (5) with finite A. According to CAK, for sufficiently large values of E, there are two solutions in the supersonic regime, $W > A^2$, termed "shallow" (small W') and "steep" (large W') solutions; whereas in the subsonic, photospheric regime, $W < A^2$, only the shallow solutions exist. On the other hand, only the steep solutions reach infinity. Namely, the term $-4A^2/U$ (the thermal pressure force caused by geometrical expansion) becomes infinite for $r \to \infty$ and must be balanced by $W' \to \infty$ along the branch of steep solutions. CAK concluded, therefore, that the true, unique wind solution has to switch from the shallow to the steep branch at a "critical" point (see Fig. 1). Of course, a nonzero pressure term at infinity is unphysical because it requires an infinite amount of energy in the flow and is purely a result of the imposed isothermal conditions in the wind.

We find that shallow solutions can always be extended to infinity, *if* one allows for a kink in the velocity law at large radii. At this kink, the wind switches to the branch of decelerating solutions, $W' < 0$. The latter are found after replacing W'^{α} in the line force by $|W'|^{\alpha}$. Since stellar winds essentially reach v_∞ at a few 100 R_*, the kink and subsequent deceleration hardly show up. For disk winds, the kink can be more pronounced; this is discussed further in Appendix B.

The subsonic region has an extent of a few percent of the stellar radius for O-star winds, while the pressure force $-4A^2/U$ becomes important only beyond a few 100 R_*. In the intermediate regime, i.e., almost everywhere, the simplified equation (7) with $A = 0$ holds to a good approximation, and therefore $W' = \text{const}$. This happens because both gravity and line force are $\propto r^{-2}$. Solution curves in the (W', U)-plane are essentially straight lines, but the lines bend over because of thermal pressure both at $U = -1$ and 0. As a result, the critical point is a saddle point in the (W', U)-plane (Bjorkman 1995). The usual definition of a critical point in hydrodynamics refers, however, to the (W, U)-plane (a topologically equivalent plane).

For $A = 0$, the critical point lies on an extended ridge, and its position becomes ill-defined (Fig. 1*a*). In this limit, *every* point of the critical solution is a critical point. For $A > 0$, however, CAK find the critical point to lie at $r_{\rm cr} = 3/2R_*$ (Fig. 1*b*). Inclusion of further correction terms to the line force, especially owing to the finite size of the stellar disk, breaks the r^{-2} dependence of the line force, pushes the two almost degenerate critical solutions $W'(U)$ apart, and shifts the critical point toward the sonic point (Fig. 1*c*). Pauldrach et al. (1986) find then $r_{\rm cr} \lesssim 1.1R_*$.

A critical point is the information barrier for LDWs and plays a role similar to the sonic point in thermal winds or nozzle flows (Abbott 1980). How can the pressure mismatch of a shallow solution at $r \gtrsim 300R_*$ be communicated upstream to the critical point at $1.1R_*$? We speculate that it is not really the outer boundary mismatch that forces the flow through a critical point. Instead, the truly distinguishing property of the critical solution should be its correspondence to the *maximum* mass-loss rate in the wind. Work is underway to identify the feedback mechanism between the wind and the photosphere that drives the wind from any shallow solution to the unique critical solution. This issue will be addressed elsewhere. In the present paper, we *assume* that the true disk wind solution is the one with the maximal allowable mass-loss rate.

The flow critical point (subscript "cr") is defined by the singularity condition, $\partial P/\partial W'_{\rm cr} = 0$ (i.e., the merging of a shallow and a steep solution). Together with the Euler equation, $P = 0$, this implies

$$W'_{\rm cr} = \frac{\alpha}{1-\alpha}\,, \tag{8a}$$

$$E_{\rm cr} = \frac{1}{\alpha^{\alpha}(1-\alpha)^{1-\alpha}}\,. \tag{8b}$$

The eigenvalue $E_{\rm cr}$ determines the maximum mass-loss rate, and $W'_{\rm cr}$ determines the terminal speed. They are discussed further in Paper II. Furthermore, from the Euler equation, $dP/dU = 0$ must hold everywhere. This leads to the regularity condition, $\partial P/\partial U_{\rm cr} + W'_{\rm cr}\,\partial P/\partial W_{\rm cr} = 0$ (if $W''_{\rm cr} < \infty$), which determines the position of the critical point.

3. DISK WIND GEOMETRY AND RADIATION FIELD IN CVS

3.1. *Flow Geometry, Gravity, and Centrifugal Force*

The central assumption throughout this paper is that the helical streamline of a fluid parcel in the wind is contained within a *straight* cone. While this is certainly an idealization, and a major restriction of this model, justification comes first from the related kinematical model of Shlosman & Vitello (1993) and second from the numerical two-dimensional hydrodynamic simulations of PSD. The latter showed that the escaping mass loss carrying streamlines are well approximated by straight lines in the (r, z)-plane, with r and z being cylindrical coordinates. The rotational speed and the centrifugal forces in the wind depend on the cone opening angle that is calculated self-consistently here. The angular momentum is preserved along any streamline (see below) and, therefore, does *not* depend on its shape.

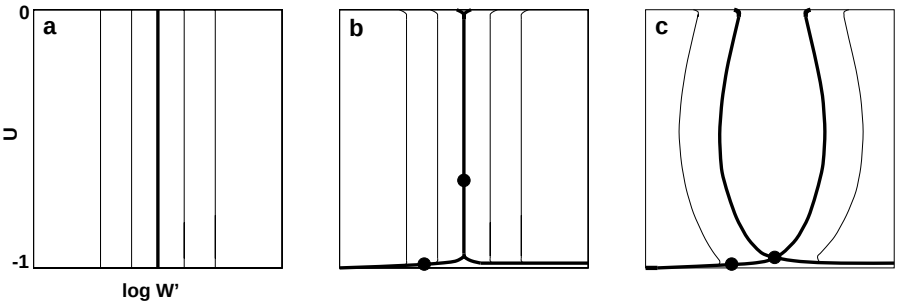

FIG. 1.—Saddle-point topology of stellar CAK winds in the (W', U)-plane, for (*a*) a point star and zero sound speed; (*b*) a point star and finite sound speed; (*c*) an extended star and finite sound speed. Filled dots mark the sonic points (at $U \simeq -1$) and the critical points.

We denote the angle between the wind cone and the radial direction in the disk plane by λ. This angle is calculated using the Euler equation and is not assumed a priori. The footpoint radius of a streamline in the disk is r_0, and x is the distance along the cone (see Fig. 2). We search for the solutions of the Euler equation in the $[\lambda(r_0), x]$-plane for a streamline starting at arbitrary r_0. The $\lambda(r_0)$ dependence leads to the appearance of a new eigenvalue problem for the disk wind, and derivation of this function is the focus of the present paper.

Since LDWs are highly supersonic, we neglect the pressure forces and furthermore assume that the azimuthal velocity is determined by angular momentum conservation above the disk and by Keplerian rotation in the disk plane. The tilt angle λ has to be a monotonically decreasing function of r_0 to avoid streamline crossing, which would violate the assumption of a pressure-free gas. The only remaining velocity component is v_x, which points upward along the cone. The dynamical problem has therefore been reduced to solving the Euler equation for v_x.

In a frame rotating with the angular velocity $\boldsymbol{\Omega}$ of a fluid parcel positioned at radius vector $\boldsymbol{s}$, there are three fictitious forces (e.g., Binney & Tremaine 1987, p. 664). The Coriolis acceleration, $-2\,\boldsymbol{\Omega} \times \dot{\boldsymbol{s}}$, has no component along $\hat{\boldsymbol{x}}$, and the same is true for the inertial force of rotation, $-\dot{\boldsymbol{\Omega}} \times \boldsymbol{s}$. We introduce the effective gravity function, which is the component of gravity minus centrifugal force along the straight line in direction $\hat{\boldsymbol{x}}$, and is given by $-(GM_{\rm wd}/r_0^2)\, g(X, \lambda)$, with $M_{\rm wd}$ being the mass of the white dwarf, and

$$g(X, \lambda) = \frac{X + \cos\lambda}{(1 + 2X\cos\lambda + X^2)^{3/2}} - \frac{\cos\lambda}{(1 + X\cos\lambda)^3}\,, \quad (9)$$

where $X \equiv x/r_0$. In the following, all lengths written in capital letters are normalized to the footpoint radius, r_0, in the disk. For disk winds, the variable X will play the role U played for stellar winds (cf. eq. [5]). Close to the disk, $X \ll 1$, and $g \simeq X$, while for $X \gg 1$, $g \simeq X^{-2}$. For a vertical ray, $\lambda = 90°$, g has its maximum at $X = 1/\sqrt{2}$, while for a horizontal ray, $\lambda = 0$, the maximum is at $X = \frac{1}{2}$.

Equation (9) shows an important difference between stellar and disk winds. The stellar gravity is always decreasing with distance, while for the disk an effective gravity "hill" must be overcome before the wind can escape. This effect of disk LDWs will be discussed in § 5.

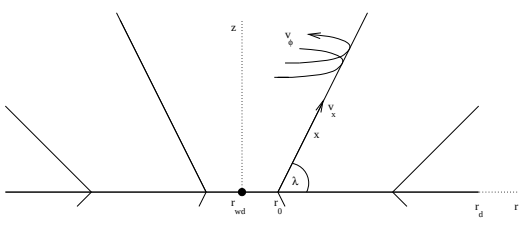

FIG. 2.—Adopted flow geometry for a CV disk wind. Streamlines are helical lines and are assumed to lie on straight cones.

3.2. *Radiation Field above the Disk*

Next, we evaluate the line force in equation (2). Besides the initial growth of effective gravity with height, the opacity-weighted flux integral is the central property that distinguishes disk winds from stellar winds. Pereyra, Kallman, & Blondin (1997) give an analytical approximation for this integral above an isothermal disk. Unfortunately, an error was introduced with a change of integration variable, which led to an artificial, linear dependence of the vertical flux on z, even as $z \to 0$. PSD solve this integral numerically (cf. Icke 1980), using approximately 2000 Gaussian integration points.

In the general spirit of the radial streaming approximation of CAK, we replace the integral in equation (2) by $\bar{\tau}^{-\alpha}\boldsymbol{F}$, thus introducing an *equivalent* optical depth, $\bar{\tau}$. We first calculate the frequency-integrated flux $d\boldsymbol{F}(r, z)$ at a location (r, z) in cylindrical coordinates, from a flat ring of radius q, radial width dq, and isotropic intensity $I(q, 0)$,

$$d\boldsymbol{F}(r, z) = \begin{pmatrix} dF_r \\ dF_z \end{pmatrix} = 2\pi I(q, 0) q\, dq\, \frac{z}{B^{3/2}} \begin{pmatrix} r[r^2 + z^2 - q^2] \\ z[r^2 + z^2 + q^2] \end{pmatrix}, \quad (10)$$

where

$$B = (r^2 + z^2 - q^2)^2 + 4z^2q^2\,. \quad (11)$$

For an *isothermal* disk with isotropic intensity, we integrate equation (10) over q, to obtain the disk flux

$$\boldsymbol{F}(r, z) = \frac{\pi I}{2}\frac{1}{\sqrt{B}} \begin{pmatrix} [z/r][r^2 + z^2 + q^2] \\ -r^2 - z^2 + q^2 \end{pmatrix}\Bigg|_{q=r_{\rm wd}}^{r_d}, \quad (12)$$

where r_d is the outer disk radius. For the nonmagnetic systems considered here, we identify the inner disk radius with $r_{\rm wd}$, the white dwarf radius. We do not include contributions to the radiative flux from the white dwarf and the boundary layer. Generally, of course, accretion disks are not isothermal. We, therefore, consider two complementary cases with $T(r_0) \propto r_0^{-1/2}$ (termed "Newtonian" disk in what follows) and $T(r_0) \propto r_0^{-3/4}[1 - (r_{\rm wd}/r_0)^{1/2}]^{1/4}$ (Shakura & Sunyaev 1973; hereafter SHS). Observations show that the brightness temperature stratification of CV disks is consis-

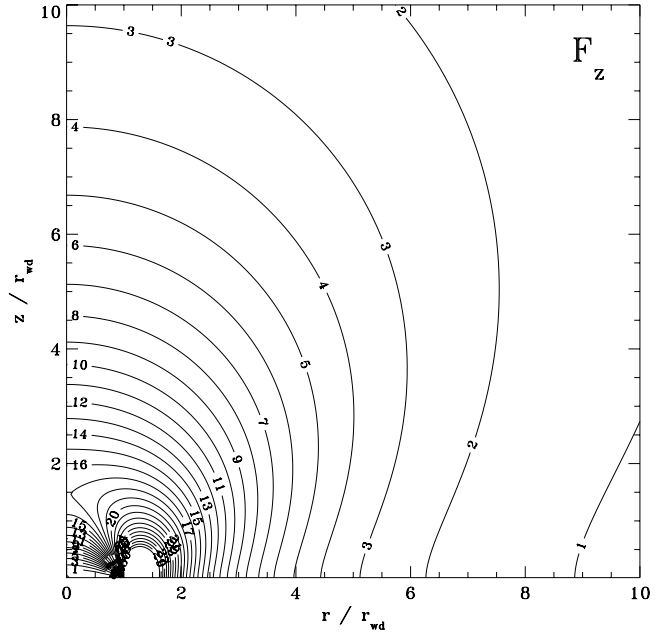

FIG. 3.—Isocontours of the frequency-integrated, vertical flux component F_z above a Newtonian disk. The disk extends from 1 to $30r_{wd}$. Normalization is $I(r_0 = 5r_{wd}, z = 0) = 1$.

tent with both distributions (Horne & Stiening 1985; Horne & Cook 1985; Rutten et al. 1993).

For the Newtonian disk, we find

$$\boldsymbol{F}(r, z) = \pi I(r, 0) r^2 \frac{z}{r^2 + z^2} \times \left(\frac{3r^2 - z^2 - q^2}{2r\sqrt{B}} - \frac{r}{z^2 + r^2} \ln C \right) \Bigg|_{q = r_{wd}}^{r_d}, \quad (13)$$

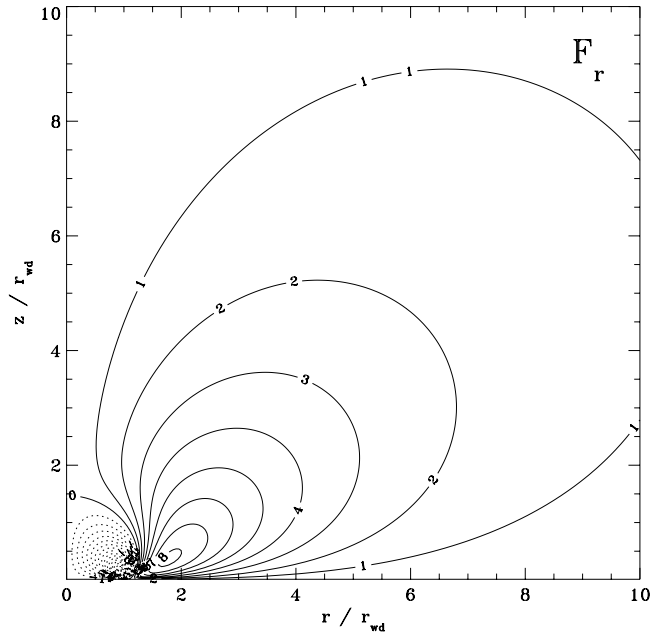

FIG. 4.—Same as Fig. 3 (including normalization), now for the radial flux component F_r. Dotted lines indicate an inward flux.

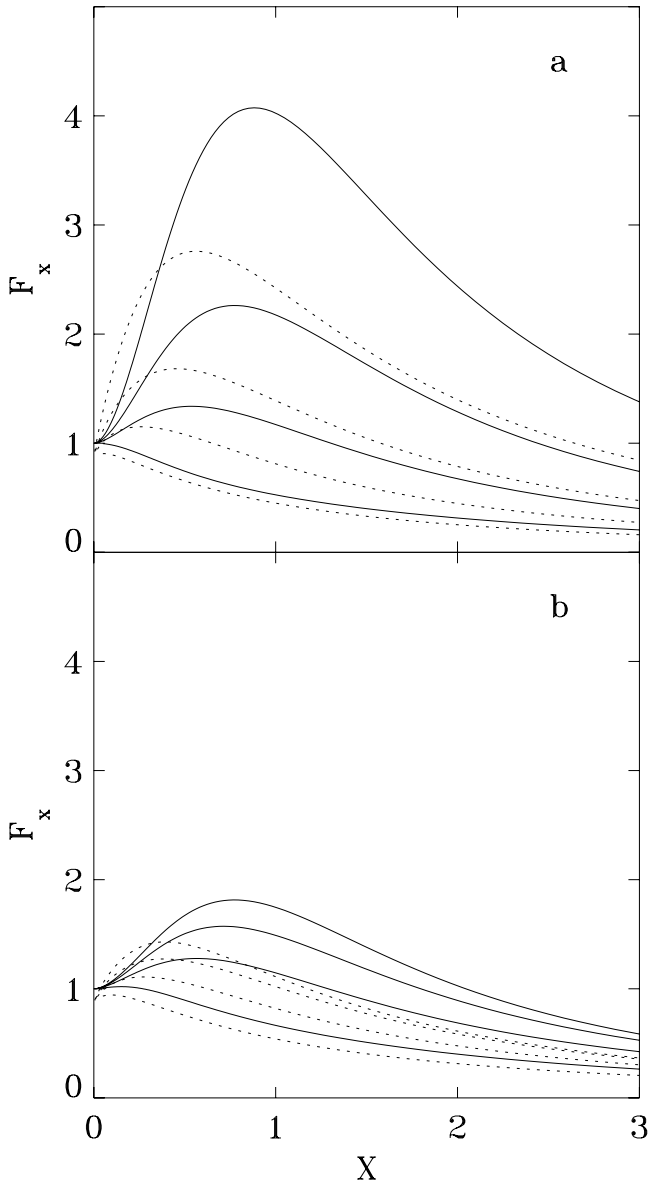

FIG. 5.—Normalized, projected flux $\tilde{F}_x(r_0, X)$ for SHS (*a*) and Newtonian (*b*) disks, at footpoint radii $r_0 = 20$, 10, 5, and $2r_{wd}$ (*top to bottom curves*). The tilt angle with the disk plane is 90° for full lines and 60° for dashed lines.

where

$$C = \frac{(z^2 - r^2)q^2 + (z^2 + r^2)^2 + (z^2 + r^2)\sqrt{B}}{q^2}. \quad (14)$$

The surface flux above the SHS disk can only be integrated numerically, using equation (10). Yet, this has the advantage that $\bar{\tau}$ can be introduced for each ring individually. More specifically, $\bar{\tau}$ is calculated along the flux direction of a given ring at the position of the wind parcel. If the flux in equation (13) is used instead, $\bar{\tau}$ is calculated along the disk flux direction. Typical differences in the resulting value for the tilt angle λ_{cr} (see below) are 5°–10° for the two approaches. Corrections owing to the $\tau^{-\alpha}$ weighting in the azimuthal integral are even smaller.

Figures 3 and 4 show isocontours for the *z*- and *r*-components of the flux in equation (13) above the Newtonian disk. For sufficiently large tilt angles, the flux along the

streamlines has a maximum larger than $\pi I(r_0, 0)$ at some X. This is caused by the increasing visibility of the inner, hot disk regions. We denote this regime, where the flux has a maximum, the "panoramic" regime, to be distinguished from the planar "disk" regime, where $F_z \simeq \pi I$, and the "far field" regime, where $F \propto X^{-2}$.

We introduce the normalized flux, $\tilde{\boldsymbol{F}}(r, z) = \boldsymbol{F}(r, z)/\pi I(r_0, 0)$, along a streamline, which is independent of disk luminosity. To quantify the flux increase above the disk, Figure 5 shows the projected, normalized flux $\tilde{F}_x = \hat{\boldsymbol{x}} \cdot \tilde{\boldsymbol{F}}$ as function of X, for different footpoint radii r_0 and for both types of nonisothermal disks. Note that the initial increase of $\tilde{F}_x$ with X caused by the wind's exposure to the central disk region is rather mild, a factor of a few only, because the central region has a small area. In § 5 we discuss how the maximum in $\tilde{F}_x$ controls the base extent of the wind above the disk, as well as the height of the wind critical point.

In deriving the above fluxes, the intensity was assumed to be isotropic. Using instead the Eddington limb darkening law, $I_\theta = 2/5 I_0[1 + (3/2) \cos \theta]$, with polar angle θ, the vertical flux in the planar disk regime above an isothermal disk becomes larger by a factor of 8/7, i.e., limb darkening should not significantly affect the wind properties. However, limb darkening can be more important in the UV spectral regime because of the Wien part of the spectrum, and the correction factors could become somewhat larger there (Diaz, Wade, & Hubeny 1996).

4. VERTICAL WIND ABOVE AN ISOTHERMAL DISK

As an analytically tractable case, we consider first a vertical (or cylindrical) wind with $\lambda = 90°$, or $\hat{\boldsymbol{x}} = \hat{\boldsymbol{z}}$, above an infinite, isothermal disk with flux $\boldsymbol{F} = \pi I \hat{\boldsymbol{z}}$. We again adopt the "radial streaming" approximation in equation (2), i.e., $\bar{\tau} = \tau_z$. Note that τ_z has no contributions from either azimuthal velocity gradients, $\partial v_\phi/\partial r$, or from geometrical expansion terms, $\propto v_\phi$, the latter describing photon escape along the tangent to the helical streamline.

The density ρ that enters τ is replaced by introducing the mass-loss rate from one side of a disk annulus, $d\dot{M}$. Since the mass that streams upward between two cylinders is conserved,

$$d\dot{M}(r_0) = 2\pi r_0 \, dr_0 \, v_x(r_0, x)\rho(r_0, x) \, . \tag{15}$$

For simplicity, we apply the zero sound speed limit, $A = 0$, for the rest of this paper and neglect the force caused by electron scattering because of small Γ above the geometrically thin disk. The Euler equation becomes

$$0 = P(W', X) = W' + g - EW'^{\alpha} \, , \tag{16}$$

where $g = X/(1 + X^2)^{3/2}$ for $\lambda = 90°$, and $W' = dW/dX = 2V \, dV/dX$. Here $d/dX = r_0 \, d/dx$, and V is the flow speed along X, normalized to the *local* escape speed at the footpoint r_0 on the disk. Note the difference in the definition of W' as compared with that for stellar winds (cf. eq. [5]). Also, normalizing the velocity V instead to the escape speed from the white dwarf leads to unwanted, explicit appearances of r_0 in the Euler equation. The constant $E(r_0)$ for a streamline starting at r_0 on the disk is defined as (cf. eq. [6])

$$E(r_0) = \frac{\Gamma(\alpha)}{1 - \alpha} \left(\frac{\kappa_0 \, v_{\rm th}}{2\pi G \, M_{\rm wd}} \right)^{1-\alpha} \frac{2\pi r_0^2 \, F_z(r_0, z = 0)/c^2}{(r_0 \, d\dot{M}(r_0)/dr_0)^{\alpha}} \, . \tag{17}$$

Similarly to the stellar case, equation (16) for the disk wind has global solutions only above a critical value $E_{\rm cr}$, the eigenvalue of the problem, i.e., below a maximum allowable mass-loss rate. Unlike the point star case, however, P in equation (16) is a function of X even when $A = 0$. As a result, the degeneracy in the position of the critical point does not exist here, and one has a well-defined critical point, irrespective of A.

There exists an additional difference between the stellar and disk LDWs. In Figure 1*c*, the finite cone correction factor causes the critical point in the stellar wind to move upstream, and, for vanishing sound speed, both the critical point and the sonic point are found in the stellar photosphere. For the disk case, however, only the sonic point falls toward the photosphere, whereas the critical point stays at finite height. Namely, from the regularity condition $\partial P/\partial X = 0$ (P does not depend on W), the critical point of the disk wind lies at the location of maximal gravity, at $X_{\rm cr} = 1/2^{1/2}$.

This explains why Vitello & Shlosman (1988) find no critical point in the disk regime, $X \ll 1$, for a vertical wind with constant ionization. The variable wind ionization introduces additional gradients into the driving force, shifting the critical point toward the disk photosphere. For the solution discussed here, vertical ionization gradients are not mandatory.

Additional justification that the critical solution is the true wind solution comes from the fact that only the shallow solutions connect to the photosphere. However, terminal speeds of the shallow solutions are much smaller than the white dwarf escape speed, in sharp contrast to observed CV winds. The solution we are searching for should, therefore, switch to the steep branch (with large v_∞) at a critical point, i.e., there should be the solution of maximum mass-loss rate.

The conditions $P = 0$ and $\partial P/\partial W' = 0$ lead to

$$W'_{\rm cr} = \frac{\alpha}{1 - \alpha} \, g_{\rm cr} \, , \tag{18a}$$

$$E_{\rm cr} = \frac{1}{\alpha^{\alpha}(1 - \alpha)^{1-\alpha}} \, g_{\rm cr}^{1-\alpha} \, , \tag{18b}$$

where $g_{\rm cr} = 2/(3 \times 3^{1/2})$. This defines the wind solution of maximum allowable mass-loss rate. The effective gravity hill imposes a "bottleneck" on the flow, i.e., the maximum of $g(X)$ defines the minimum, constant eigenvalue $E_{\rm cr}$, or the maximum allowable $\dot{M}$, for the critical solution which extends from the disk photosphere to large X. Larger values of E correspond to shallow solutions and, hence, to smaller mass-loss rates. Smaller values of E correspond to stalling wind solutions, which become imaginary around the location of the gravity maximum. Note that $E_{\rm cr}$ in equation (18b) is independent of r_0, in accordance with equation (16).

5. TILTED DISK WINDS

With all prerequisites at hand, we can now solve the general eigenvalue problem for a tilted wind above a nonisothermal disk. The density ρ in equation (3) is replaced by the conserved mass-loss rate between two wind cones,

$$d\dot{M}(r_0) = 2\pi r_0 \, dr_0 (1 + X \cos \lambda) \times \left[1 - \frac{X r_0 \, (d\lambda/dr_0)}{\sin \lambda} \right] \sin \lambda v_x(r_0, x)\rho(r_0, x) \, . \tag{19}$$

The term $(1 + X \cos \lambda)$ describes the density drop caused by the increasing radius of the cone, and $[1 - Xr_0 (d\lambda/dr_0)/\sin \lambda]$ describes the density drop caused by the geometrical divergence of neighboring cones. The factor $\sin \lambda$ stems from the quenching of the flow at small λ.

5.1. *Disk Euler Equation*

The geometrical expansion term $\nabla\hat{\gamma}$ in the directional derivative $\hat{\gamma} \cdot \nabla(\hat{\gamma} \cdot \mathbf{v})$ has contributions from the azimuthal curvature of helical streamlines and from the cone divergence $d\lambda/dr_0$. *Close* to the disk, where the mass-loss rate of the wind is established, both contributions are small. For azimuthal curvature terms, this is shown in Appendix A. With regard to cone divergence, the argument is a posteriori, i.e., we find below that $d\lambda/dr_0$ is small. Two neighboring wind rays launched at, e.g., $r_0 \sim 5r_{\rm wd}$ intersect at a normalized distance $X_i \sim -10$ below the disk. Generally, X_i is larger by a factor of 10 than $X_{\rm cr}$, the distance between the disk and the critical point. By analogy with spherically symmetric stellar winds, where $\hat{\gamma} \cdot \nabla(\hat{\gamma} \cdot \hat{\mathbf{r}} v_r) = \mu^2 \, dv_r/dr + (1 - \mu^2)v_r/r$, with $\mu = \hat{\gamma} \cdot \hat{\mathbf{r}}$, the geometrical expansion term $\propto v_x \nabla(\hat{\gamma} \cdot \hat{\mathbf{x}})$ for disk winds should be $\propto v_x/[r_0(X - X_i)]$. Whereas the geometrical expansion term for O-star winds, $(1 - \mu^2)v_r/r$, is of the same order as the gradient term, $\mu^2 dv_r/dr$, it is much smaller than the latter for disk winds. On the other hand, *far* from the disk, the expansion term may become important. However, we find from solving the Euler equation that it has only a marginal influence on the terminal wind velocity. Furthermore, azimuthal terms for helical streamlines are unimportant far from the disk, where the wind is essentially radial. We, therefore, neglect all geometrical expansion terms in the following. Appendix A also shows that *gradients* in the azimuthal velocity can be neglected in the line force. Finally, we assume that the gradient of v_x points in the $\hat{\mathbf{x}}$-direction. This is a reasonable assumption since the velocity gradients develop roughly in the flux direction, as is shown below. The normalized Euler equation for a conical disk wind, and for vanishing sound speed, is then

$$0 = P(W', X) = W' + g - Ef W'^{\alpha} , \tag{20}$$

with auxiliary function f,

$$f(r_0, X) \equiv \left[(1 + X \cos \lambda) \left(\sin \lambda - X r_0 \frac{d\lambda}{dr_0} \right) \right]^{\alpha} \int_{r_{\rm wd}}^{r_d} d\tilde{F} \mu^{1+2\alpha} . \tag{21}$$

Here, $d\tilde{F} = |d\tilde{\boldsymbol{F}}|$ (see eq. [10]), and μ is the cosine of the angle between $d\tilde{\boldsymbol{F}}$ and the wind cone. Again, $W' = 2V \, dV/dX$, where the velocity V is normalized to the local escape speed; $E(r_0)$ is defined in equation (17). Note that the flux integral in equation (21) introduces a further dependence of f on r_0. Furthermore, because of the weighting with $\mu^{2\alpha}$ in the integral, the disk flux vector and the wind cone generally do not point in the same direction. For disk winds as considered here, good alignment between radiative flux and wind flow is expected, however. In cases where such an alignment is not possible, e.g., for atmospheres irradiated from above, *ablation* winds at large tilt angle with the radiative flux were recently suggested (Gayley, Owocki, & Cranmer 1999).

5.2. *Wind Tilt Angle as an Eigenvalue and Solution Topology*

The critical-point conditions for a specific streamline are, from equation (20)

$$W'_{\rm cr} = \frac{\alpha}{1 - \alpha} g_{\rm cr} , \tag{22a}$$

$$E_{\rm cr} = \frac{1}{\alpha^{\alpha}(1 - \alpha)^{1-\alpha}} \frac{g_{\rm cr}^{1-\alpha}}{f_{\rm cr}} , \tag{22b}$$

$$0 = (1 - \alpha) \frac{g'_{\rm cr}}{g_{\rm cr}} - \frac{f'_{\rm cr}}{f_{\rm cr}} , \tag{22c}$$

where $g' = \partial g/\partial X$ and $f' = \partial f/\partial X$. The tilted disk wind is essentially a two-dimensional phenomenon; hence, we expect two eigenvalues of the Euler equation with respect to E and λ. Finding the critical solution of maximum mass loss at a given footpoint r_0 implies minimizing E in equation (22b) with respect to the position of the "critical" point $(X_{\rm cr}, \lambda_{\rm cr})$. We show now that $(X_{\rm cr}, \lambda_{\rm cr})$ is a *saddle* point of $g^{1-\alpha}/f$. We consider first the X coordinate and recall from the analysis of the vertical disk wind that the maximum of $g^{1-\alpha}$ has determined the eigenvalue $E_{\rm cr}$. From equation (22b), the relevant function now is $g^{1-\alpha}/f$. This means that the maximum of $g^{1-\alpha}/f$ with respect to X for a fixed λ serves as a bottleneck of the flow, i.e., the most stringent condition on the wind between the photosphere and infinity. Therefore, it defines the maximum allowable mass-loss rate. Next, we analyze the mass-loss rate along a streamline by varying its tilt angle λ. To obtain the maximum mass-loss rate, we look for the minimum of $g^{1-\alpha}/f$ as a function of λ. This particular $\lambda_{\rm cr}$ plays the role of a second eigenvalue of the Euler equation, besides $E_{\rm cr}$. Note that because of the dependency of f on r_0, the wind tilt will change with r_0. The eigenvalue $E_{\rm cr}$ is thus given by

$$E_{\rm cr} = \frac{1}{\alpha^{\alpha}(1 - \alpha)^{1-\alpha}} \min_{\lambda} \max_{X} \frac{g^{1-\alpha}}{f} . \tag{23}$$

This is the definition of a saddle point of $g^{1-\alpha}/f$. Isocontours of this function are shown in Figure 6 for the SHS disk. The existence of the saddle point in $g^{1-\alpha}/f$ underlines the two-dimensional nature of disk LDWs. Because the saddle opens in the X-direction, the wind escapes to large X.

Furthermore, the critical solution of maximum mass loss passes also through a saddle point of the Euler function P in the (W', X)-plane, in complete analogy with O-star winds. (It may be an interesting task to consider the solution topology in the three-dimensional space spanned by $[\lambda, X, W']$.) The regularity condition, equation (22c), determines the loci $X_{\rm cr}$ of these critical points, as shown by the heavy lines in Figure 6. On the left branch of these curves, which also pass through the saddle point of $g^{1-\alpha}/f$ (if the latter exists), lie critical points of the saddle- or X-type. Here, $W'(X)$ can switch from a shallow (small W') to a steep (large W') solution. On the other hand, the right branch of the regularity curves, which pass through the minimum of $g^{1-\alpha}/f$, consists of critical points of the focal type (Holzer 1977; Mihalas & Mihalas 1984). They correspond to solutions that do not extend from the disk photosphere to large radii and are ignored in our discussion.

Figure 7 shows a good overall alignment of the wind ray of maximum mass-loss rate with the radiative flux vector from the disk, at least up to the critical point. This is (1)

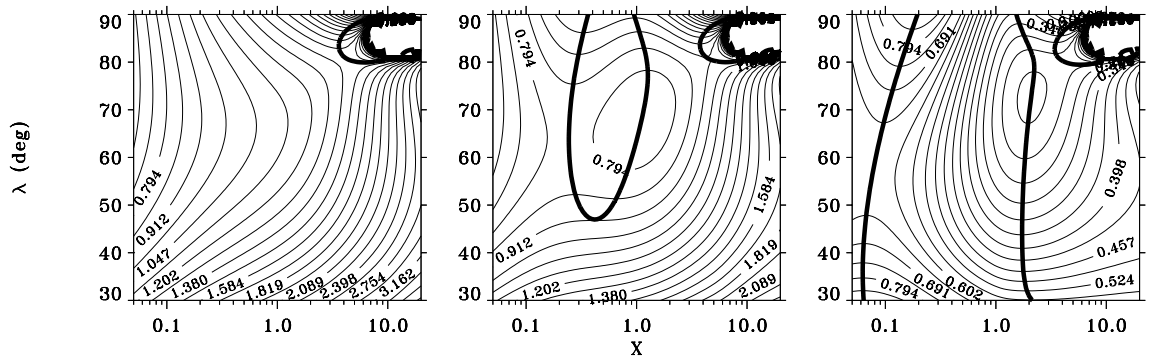

FIG. 6.—Isocontours of $g^{1-\alpha}/f$, normalized to $[2/(3 \times 3^{1/2})]^{1-\alpha}$, over the (X, λ)-plane. Footpoints of the wind are at $r_0 = 3$, 5, and $15 r_{wd}$, respectively (*left to right panels*). The isocontours have logarithmic spacing. The temperature stratification is that of the SHS disk with $r_d = 30 r_{wd}$, and $\alpha = \frac{2}{3}$ was used. Heavy lines are solutions to the regularity condition in eq. (22c).

because the eigenvalue E_{cr} depends linearly on f, but only with a small power of $1 - \alpha$ on g, and (2) because only $f(\lambda)$ has a maximum, whereas $g(\lambda)$ falls off monotonically.

The figure suggests that the wind should actually be launched vertically from the disk surface and then later bend over because of the increasing radial flux component. The latter is (mostly) caused by the radial temperature stratification of the disk, $T \propto r_0^{-n/4}$, with some number n. From a series expansion, one finds $F_r(z) \propto -nz \ln z$, for $z \ll r_0$. We expect streamline bending because of this initial increase in F_r to be more important than bending caused by the higher gas pressure at smaller radii (for a disk with radial temperature fall-off). Furthermore, streamline bending caused by centrifugal forces occurs only on a much larger length scale, r_0. Since the true bent trajectory is expected to follow the flux vector rather closely, a somewhat larger mass-loss rate is expected than along straight wind cones. However, the difference should be rather small. A clear benefit from this approximation is a dramatically reduced complexity of the wind treatment.

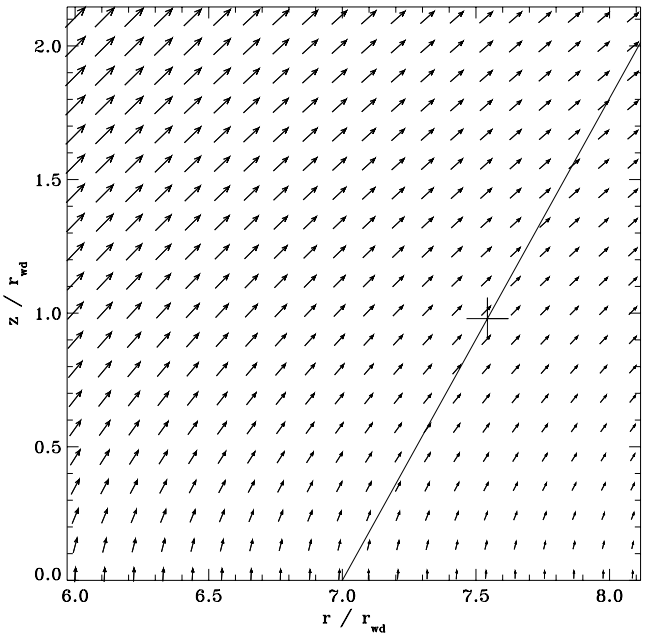

FIG. 7.—Radiative flux vector above the SHS disk with $r_d = 30 r_{wd}$. The straight line indicates a wind cone at eigenvalue $\lambda = 61°$ (cf. Table 1). The plus sign marks the critical point.

5.3. *Inner and Outer Disk Winds*

Up to this point we ignored the possibility of multiple saddle points of $g^{1-\alpha}/f$. We now address this issue. As shown in Figure 6, for $r_0 \lesssim 4 r_{wd}$ the function $g^{1-\alpha}/f$ has only one saddle at a large height, e.g., $X_{cr} \simeq 4.4$ for $\alpha = \frac{2}{3}$. However, for $r_0 \gtrsim 4 r_{wd}$, a second saddle exists at smaller X_{cr}, which lies on a different branch of the regularity curve. We name these two types of saddles the *high* and *low* saddles, according to their height X_{cr} above the disk. The effective gravity "hill" separates the two saddle points.

From Figure 6, the low saddle corresponds to a larger mass-loss rate than does the high saddle. For $r_0 \gtrsim 4 r_{wd}$, the solution of maximum mass loss is therefore determined by the low saddle. For smaller r_0, however, only the high saddle exists and determines the wind solution. These two cases define the *outer* and *inner* disk wind, respectively. Clearly, the assumption of straight streamlines is a severe one for the inner wind with high-lying critical points.

The tilt angle of the outer wind is around 60°, namely $\lambda_{cr} = 65°$ at $r_0 = 4 r_{wd}$, and 55° at 20 r_{wd}. This is largely independent of α. For the inner wind, the tilt is larger, $\lambda_{cr} = 80°$ for $\alpha = \frac{2}{3}$ and 70° for $\alpha = \frac{1}{2}$. Furthermore, the critical point, X_{cr}, for the inner wind is much higher above the disk than the critical point for the outer wind. As mentioned above, these critical points fall on the opposite slopes of the effective gravity hill. For the outer disk wind, the position X_{cr} of the critical point is moving closer to the wind sonic point with increasing r_0. The reason for this is the larger gradient of the disk radiative flux in the x-direction for larger r_0. As a result, the line force can balance gravity at smaller X.

Figure 8 shows critical wind solutions $W'(X)$ above the SHS disk for different r_0. The decelerating solution branches, $W' < 0$, are discussed in Appendix B. The critical point topology of Figure 8 may be compared with that of the CAK stellar wind in Figure 1. (Note, that W' has a slightly different definition for the stellar and disk wind cases.) From Figure 8, we can also derive a condition for the *existence* of a stationary, outer wind solution, further clarifying the role of the effective gravity hill. The plus signs at the critical points in the figure indicate where the Euler function $P > 0$, i.e., where drag forces (gravity and inertia) overcome the driving forces (line and centrifugal force); this is correspondingly so for the minus signs. Hence, $\partial^2 P/\partial X_{cr}^2 < 0$ at the low saddle, or, using equation (22a), (22b), and (22c), $(1 - \alpha)\, g''_{cr}/g_{cr} < f''_{cr}/f_{cr}$ (respectively, " > "

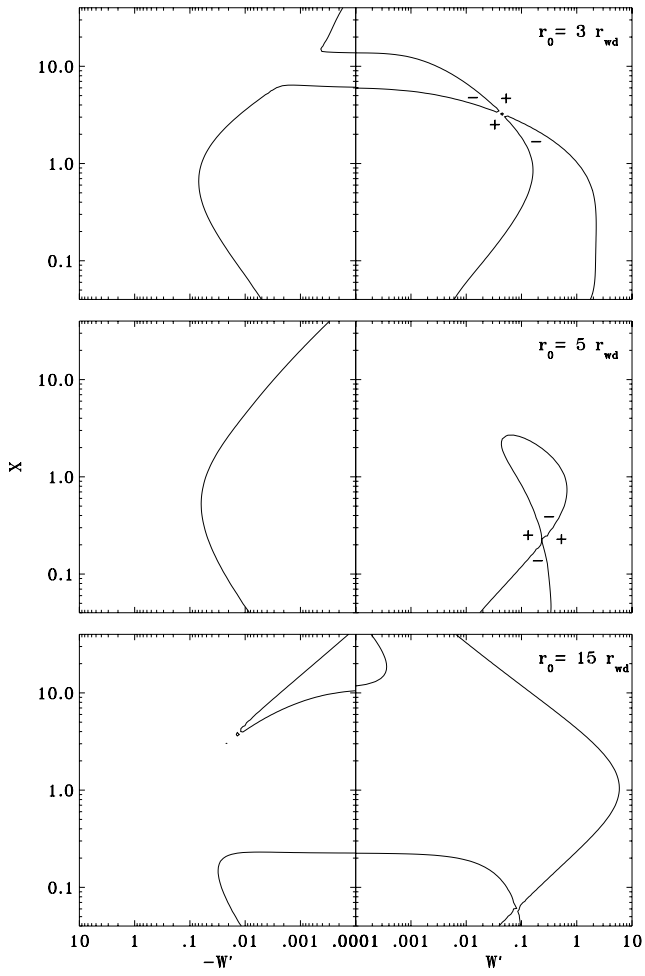

FIG. 8.—Critical wind solutions $W'(X)$ at zero sound speed above the SHS disk ($r_d = 30r_{wd}$, $\alpha = \frac{2}{3}$). At $r_0 = 3r_{wd}$: *high* saddle; at $r_0 = 5$ and $15r_{wd}$: *low* saddle. The branches $W' < 0$ are decelerating wind solutions and are discussed in Appendix B. Plus and minus signs refer to the sign of the Euler function P in eq. (20). For comparison with the critical-point topology of a spherically symmetric, stellar wind, see Fig. 1.

at the high saddle). This means, the maximum of f must be sufficiently broad to allow for a stationary solution with a low saddle. The critical point for a vertical wind above an infinite, isothermal disk, where $f = 1$, corresponds to a low saddle.

To understand the geometry of disk LDWs fully, we consider also the transition region between the inner and outer winds. As discussed above, the low saddle does not exist below $r_0 \lesssim 4r_{wd}$. Figure 9 shows $g^{1-\alpha}/f$ in the neighborhood of this footpoint radius. At $r_0 = 4r_{wd}$, only the high saddle exists and determines the wind solution. At $r_0 = 4.03r_{wd}$, an inner regularity curve of elliptical shape has formed but not yet the low saddle point of $g^{1-\alpha}/f$. The mass-loss rate is maximal at the smallest λ along the curve, i.e., at its lower tip, which determines the wind solution in this transition regime. By $r_0 = 4.15r_{wd}$, a low saddle has formed at $\lambda_{cr} = 65°$. Going to larger r_0, the wind tilt stays (roughly) at this value λ_{cr}, which corresponds to the maximum mass-loss rate. In total, the wind tilt switches continuously from the high to the low saddle over a narrow range of $0.1\ r_{wd}$ in the footpoint radius.

5.4. *Overall Disk Wind Geometry*

Table 1 lists important parameters of the wind above SHS and Newtonian disks, i.e., the tilt angle, λ_{cr}, the normalized mass-loss rate from a disk annulus, $\dot{m}_{cr}$, and the critical point location, X_{cr}. The mass-loss rate $\dot{m}$ is normalized to a vertical wind above an isothermal disk. The shallow maxima of the function $\tilde{F}_x$ in Figure 5 are responsible for $\dot{m} = O(1)$. Implications of these mass-loss rates are discussed in Paper II. From the table, one finds the ray dispersion in the outer wind, at intermediate footpoint radii 4–10 r_{wd}, to be

$$\frac{d\lambda}{dr_0} \simeq -\frac{1°}{r_{wd}}\,. \tag{24}$$

Farther in or out, the ray dispersion is even smaller. Since $d\lambda/dr_0$ also enters the Euler equation (20), the full wind problem can be solved only iteratively. However, the dependence of the eigenvalues E_{cr} and λ_{cr} on $d\lambda/dr_0$ is weak, and we assume throughout that equation (24) holds.

The overall geometry of the disk wind is shown in Figure 10. For $\alpha = \frac{2}{3}$, the critical points are at $x_{cr} \sim 10$–$20\ r_{wd}$ for the inner wind, then move toward the disk photosphere and stay at $x_{cr} \simeq r_{wd}$, independent of footpoint radius r_0 in the outer wind. For $\alpha = \frac{1}{2}$, on the other hand, the critical points lie somewhat higher for the outer wind, at $x_{cr} \simeq 2r_{wd}$, but their location is again independent of radius r_0. While the division into an inner and outer wind persists (namely high-lying vs. low-lying saddle, or critical points on opposing

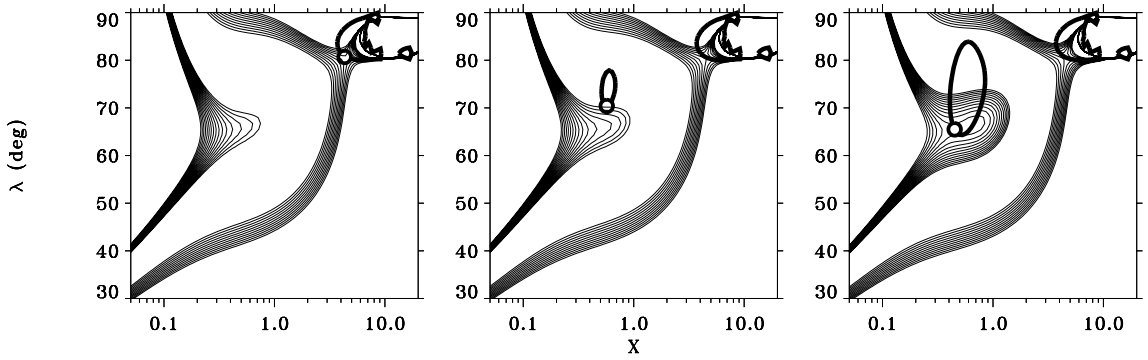

FIG. 9.—Isocontours of $g^{1-\alpha}/f$, normalized to $(2/3\sqrt{3})^{1-\alpha}$; from 0.855 to 0.885 in steps of 2×10^{-3} at the low saddle; from 1.05 to 1.15 in steps of 10^{-2} at the high saddle. At $r_0 = 4$, 4.03, and $4.15r_{wd}$, respectively (*left to right panels*). Heavy lines are solutions to the regularity condition. Circles mark the critical wind solution of maximum mass-loss rate. Within the footpoint range from $r_0 = 4$ to $4.15r_{wd}$, the wind switches from $\lambda_{cr} = 80°$ to $\lambda_{cr} = 65°$ via a growing regularity curve of ellipsoidal shape.

TABLE 1

TILT ANGLE λ_{cr}, NORMALIZED MASS-LOSS RATE $\dot{m}_{cr}$, AND POSITION X_{cr} OF THE CRITICAL POINT FOR DIFFERENT DISK WIND MODELS

	SHS Disk						Newtonian Disk					
	$\alpha = \frac{2}{3}$			$\alpha = \frac{1}{2}$			$\alpha = \frac{2}{3}$			$\alpha = \frac{1}{2}$		
r_0/r_{wd}	$\lambda_{cr}(^\circ)$	$\dot{m}_{cr}$	X_{cr}	λ_{cr}	$\dot{m}_{cr}$	X_{cr}	λ_{cr}	$\dot{m}_{cr}$	X_{cr}	λ_{cr}	$\dot{m}_{cr}$	X_{cr}
2.....	80	0.42	4.4	68	0.62	1.9	78	0.64	4.3	65	0.94	1.2
3.....	80	0.60	4.4	72	1.02	2.3	78	0.90	4.7	65	1.45	0.82
4.....	80	0.86	4.4	69	1.60	1.7	65	1.23	0.32	63	1.78	0.58
5.....	64	1.37	0.26	63	2.23	0.52	64	1.32	0.26	62	2.10	0.43
6.....	62	1.48	0.19	61	2.69	0.35	63	1.37	0.23	61	2.23	0.38
7.....	61	1.60	0.16	60	3.08	0.27	63	1.37	0.21	61	2.37	0.34
10.....	58	1.82	0.11	58	3.84	0.18	62	1.48	0.17	60	2.69	0.28
15.....	57	2.10	0.08	55	5.41	0.12	61	1.54	0.15	58	3.08	0.23
20.....	56	2.26	0.06	53	6.57	0.10	60	1.60	0.13	58	3.31	0.2
25.....	55	2.45	0.05	52	8.16	0.08	60	1.67	0.13	57	3.31	0.3
28.....	55	2.59	0.04	51	8.16	0.10	58	1.35	0.2	57	2.44	0.2

NOTE—.Underlined numbers indicate the transition from the inner to the outer wind.

sides of the gravity hill), the transition in λ between the two regions is smooth for $\alpha = \frac{1}{2}$, and the inner tilt reaches a maximum of $\lambda = 70^\circ$ only.

The innermost disk region, from 1–$2r_{wd}$, is left out of Figure 10. The details of the disk wind and its very existence here are subject to great uncertainties in the radiation field, which depends on the properties of the transition layer and the white dwarf itself. The outer boundary of the disk LDW, on the other hand, is set by the radius where the disk temperature falls below 10^4 K and UV line driving becomes inefficient, in analogy with stellar winds (Abbott 1982; Kudritzki et al. 1998). For the SHS disk with $L_d = 10\ L_\odot$, this should happen around $30r_{wd}$.

6. DISCUSSION

Here we compare our theoretical model of LDWs from accretion disks in CVs with those available in the literature, both kinematical and dynamical models. We ignore the radial wind models, with the white dwarf being the wind base, because they are in a clear contradiction with current observations (e.g., review by Mauche & Raymond 1997). An alternative source of gas is the disk itself. Kinematical models that account for this source of material subject to the line-driving force successfully explained the observed bipolarity of the outflow and reproduced the inclination-dependent line profiles (Shlosman & Vitello 1993). Their weak point was the absence of a unique solution. The one-dimensional dynamical models in a simplified disk radiation field revealed some major differences between the stellar and disk winds, e.g., the bipolarity and the existence of a gravity hill (Vitello & Shlosman 1988).

More sophisticated two-dimensional kinematical models, supplemented with a three-dimensional radiation transfer in Sobolev approximation, showed the importance of rotation in shaping the lines (Vitello & Shlosman 1993; Shlosman et al. 1996). Finally, the two-dimensional hydrodynamical model of a disk wind in a realistic radiation field and with the line-force parameterized by the CAK approximation has addressed the issue of flow streamlines and mass-loss rates in the wind (PSD). Our comparison, therefore, is focused on these models.

Vitello & Shlosman (1993) set up a kinematical disk wind model assuming straight flow lines in order to fit the C IV P Cygni line profiles of three CVs observed with the *IUE* satellite. The fit parameters included the inner and outer terminating radius of the wind base and the corresponding tilt angles of the wind cone. The best fit appeared to be *indifferent* to the mass-loss rate, within the range of 10^{-1} to 10^{-2} of the accretion rate. In the present work, which accounts for wind dynamics, we find lower mass-loss rates

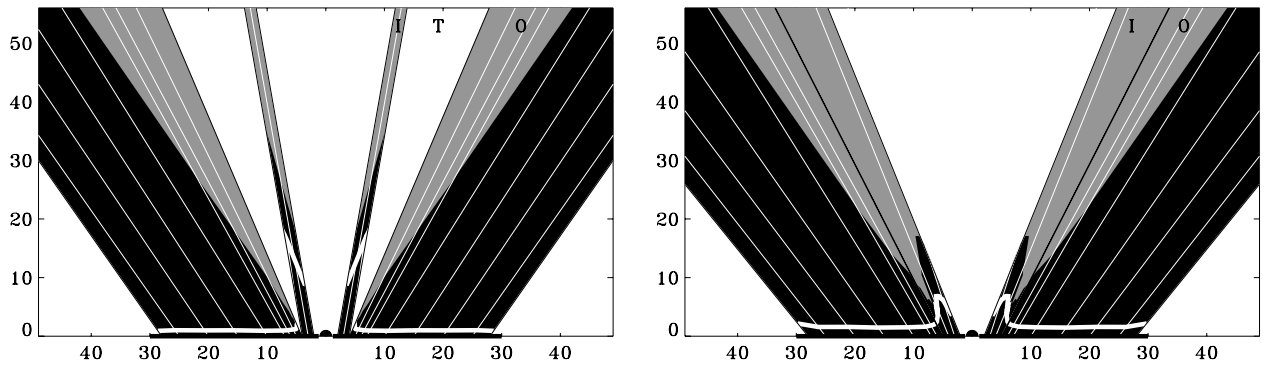

FIG. 10.—Wind geometry above the SHS disk ($r_d = 30r_{wd}$) according to Table 1, for $\alpha = \frac{2}{3}$ (*left-hand panel*) and $\alpha = \frac{1}{2}$ (*right-hand panel*). Black regions indicate the accelerating LDW, and thin white lines show individual wind cones. Gray areas indicate decelerating wind (Appendix B) for a ray dispersion $d\lambda/dr_0 = -1^\circ/r_{wd}$. "I" and "O" mark the inner and outer wind; "T" is the transition region. Heavy white lines are locations of flow critical points. The innermost region of the disk, at $r_0 < 2r_{wd}$, is not treated because of uncertainties in the radiation field.

more justified and discuss various implications of these rates on the wind models in Paper II. The tilt of the innermost wind cone in Vitello & Shlosman was rather steep, $\lambda = 80°$, while at the outer disk edge $\lambda = 25°$. A similar work by Knigge et al. (1995), but using Monte Carlo radiation transfer in the wind, gave similar results. In the present work, the tilt angle λ is calculated self-consistently from the Euler equation, resulting in a similar inner tilt as found in kinematical models, while the outer tilt differs by a factor of 2 between the two approaches.

The most advanced numerical modeling of CV winds from the SHS disk was performed by PSD using the time-dependent ZEUSS two-dimensional code. We find a number of similarities with PSD, but differences exist as well. Our comparison is limited to their models 2–5, i.e., those without a central luminous star. These models are in agreement with the overall wind geometry discussed here. This includes the streamline shape and the run of the wind opening angle with radius. The streamlines in PSD appear to form straight lines in the (r, z)-plane, in striking similarity with the previous kinematical models. In addition, the change in the wind opening angle with distance from the rotation axis seems to be weak in PSD. The mass-loss rates are consistent between both models, and so are the wind optical depths, which can approach unity even for very strong resonance lines (Paper II).

While PSD also find two markedly distinct flow regions, the inner and outer, their inner wind, at $r_0 \lesssim 4r_{\rm wd}$, appears as the only outflow. The outer disk region, at radii $\gtrsim 4r_{\rm wd}$, exhibits a time-dependent irregular flow, resulting in essentially no mass loss. On the other hand, in our model, mass loss from the SHS disk is dominated by the inner wind and the innermost part of the outer wind, as is discussed in Paper II. Interestingly, our outer wind seems to be more robust than the inner wind. For the inner wind, the balance of driving and drag forces that leads to a high saddle on the far side of the gravity hill is a rather delicate one. Setting, for example, the centrifugal force *arbitrarily* to zero causes the high saddle solution to vanish, whereas the low saddle remains almost unchanged.

PSD suggest that the irregular behavior of their outer flow is a consequence of the different X-dependence of gravity and disk flux, with the gravity preventing the wind from developing. This is similar to chocking a nozzle flow. However, we find here that at radii $r_0 \gtrsim 4r_{\rm wd}$, where a low saddle exists, the fast increase in the projected disk flux, $\tilde{F}_x(X)$, results in a sufficiently strong growth of the line force, which drives the wind past the gravity hill. For the inner wind regions, on the other hand, where no lower saddle branch exists, the wind indeed must overcome the gravity barrier without the appropriate radiation flux increase with X. In contrast to the findings of PSD, mass overloading seems therefore more likely for the inner wind. Indeed, from the simulations by PSD, it appears that wave-like perturbations originate at the base of the *inner* wind (D. Proga, 1999, private communication) and propagate to outer disk regions where they prevent a stationary solution from developing. Future work will have to clarify this issue.

Furthermore, we cannot confirm the dependence of λ on the disk luminosity as in the PSD model. We find that the eigenvalue $\lambda_{\rm cr}$ for each streamline is determined from the positions of the saddle points of the function $g^{1-\alpha}/f$. Both g and f are independent of the disk luminosity, f specifically so because it is normalized to the flux at the streamline footpoint (eq. [21]). Therefore, $\lambda_{\rm cr}$ depends only on the radial temperature stratification in the disk.

One important issue neglected in our modeling is the saturation of the line force when all the driving lines become optically thin. If this thick-to-thin transition occurs before the flow reaches its critical point, the wind solution is lost, since the drag forces overcome the driving forces. However, this still leaves the possibility that a more complicated wind dynamics is established, where the decelerating flow at some larger radius starts again to accelerate (i.e., jumps from a W'_- to a W'_+ solution). We leave this question open for future scrutiny and note here that the mass-loss rates derived from the present eigenvalues E are upper limits.

The present work is based on the CAK theory for stellar winds. Over the years, questions have been raised concerning the physical meaning of the CAK critical point (Thomas 1973; Lucy 1975; Cannon & Thomas 1977; Abbott 1980; Owocki & Rybicki 1986; Poe, Owocki, & Castor 1990). Most interesting for the present context is the inclusion of higher order corrections to the diffuse line force in the Sobolev approximation, which shift the critical point even closer to the sonic point (Owocki & Puls 1998; see also Fig. 1). This proximity of the sonic and critical points may not be coincidental, and one can speculate whether or not the *sonic* point determines the mass-loss rate instead of the critical point. In contrast, we find for the disk wind cases, where the sonic and critical points lie far apart, e.g., for a vertical wind above an isothermal disk or a tilted wind close to the rotation axis ("inner wind").

These fundamental issues impair our understanding of LDWs from stars and disks and therefore must be addressed in the future.

7. SUMMARY

We discuss an analytical model for two-dimensional stationary winds from accretion disks in cataclysmic variable stars. The parameters chosen are typical for high-accretion rate disks in nova-like CVs. We solve the Euler equation for the wind, accounting for a realistic radiation field above the disk, which drives the wind by means of radiation pressure in spectral lines. Some key assumptions are that each helical streamline lies on a straight cone; that the driving line force can be parameterized according to CAK theory; and that the thermal gas pressure in the supersonic wind can be neglected. Our results are summarized as follows.

The disk wind solutions are characterized by two eigenvalues, the mass-loss rate and the flow tilt angle, $\lambda_{\rm cr}$, with the disk. The additional eigenvalue $\lambda_{\rm cr}$ for each streamline reflects the two-dimensional nature of the model. We find that the wind exhibits a clear biconical geometry with a small ray dispersion. Specifically, two regions can be distinguished in the wind, launched from within and outside 4 $r_{\rm wd}$, respectively. The tilt angle for the outer wind is $\lambda \sim 60°$ with the disk. At these angles, the wind flow and radiative flux vectors from the disk are well aligned. For the inner wind, the tilt angle is larger, up to 80°. We emphasize that the disk wind tilt angle (i.e., the wind collimation) depends upon the radial temperature stratification in the disk solely, unless there is an additional degree of freedom such as central luminosity associated with nuclear burning on the surface of the white dwarf.

A major distinction between stellar and disk winds is the existence of maxima in both the gravity and the disk flux along each streamline. The flux maximum appears to be a

crucial factor in allowing the wind to pass over the gravity "hill." The flux increase is more pronounced farther away from the rotation axis. As a result, the critical point of the outer wind lies close to the disk photosphere and to the sonic point. In fact, it lies upstream of the top of the gravity hill, and this proximity of the critical and sonic points is typical of LDWs from O stars as well. On the other hand, for the inner wind, the increase in radiation flux with height is smaller, and the critical point lies far away from the sonic point, beyond the top of the gravity hill.

Comparing our analytical models with the two-dimensional numerical simulations of Proga et al. (1998), we find an overall good agreement in the streamline shape, tilt angle, and mass-loss rate, but our wind baseline is wider.

We are grateful to Jon Bjorkman, Rolf Kudritzki, Chris Mauche, Norman Murray, Stan Owocki, Joachim Puls, and Peter Vitello for numerous discussions on various aspects of line-driven winds. I. S. acknowledges the hospitality of the IGPP/LLNL, where this work was initiated, and of its director, Charles Alcock. This work was supported in part by NASA grants NAG5-3841 and WKU-522762-98-06, and HST GO-06546.02-95A and AR-07982.01-96A.

APPENDIX A

LINE FORCE CAUSED BY GRADIENTS IN THE AZIMUTHAL VELOCITY

We estimate here the importance of azimuthal velocity terms for the line force in the x-direction. Assuming Keplerian rotation within the disk, and angular momentum conservation above the disk, one has (with r and z being cylindrical coordinates),

$$\frac{\partial v_\phi/\partial z}{\partial v_x/\partial x} = -\frac{1}{\sqrt{2}}\,\frac{1}{\tan\lambda}\,\frac{1}{1+X\cos\lambda}\,\frac{\sqrt{W}}{W'}\,,$$

$$\frac{\partial v_\phi/\partial r}{\partial v_x/\partial x} = -\frac{1}{\sqrt{2}}\,\frac{1-X\cos\lambda}{(1+X\cos\lambda)^2}\,\frac{\sqrt{W}}{W'}\,,$$

$$-\frac{v_\phi/r}{\partial v_x/\partial x} = -\frac{\sqrt{2}}{(1+X\cos\lambda)^2}\,\frac{\sqrt{W}}{W'}\,. \tag{A1}$$

Here, the singularity of $\tan^{-1}\lambda$ at $\lambda = 0$ is a result of neglecting the pressure terms in the Euler equation. Note that $\partial v_\phi/\partial r$ changes sign at $X = 1/\cos\lambda$. From equation (A1), gradients in v_ϕ are comparable to gradients in v_x when $W^{1/2}/W' \sim 1$. The main question is their influence on the mass-loss rate. Because, in the CAK model, $\dot{M}$ is determined by the conditions at the critical point, we calculate $W^{1/2}/W'$ at the latter. We consider first a vertical wind from an isothermal disk. Since W' grows monotonically up to and somewhat beyond the critical point (see Fig. 8), and because $W = \int W'dX$, one has $(W_{\rm cr})^{1/2}/W'_{\rm cr} < (3/2)^{3/4} \times (1-\alpha/\alpha)^{1/2} \sim 1$. Here, $X_{\rm cr} = 1/2^{1/2}$ and equation (18a) were used. Alternatively, the critical points of the outer wind above a nonisothermal disk typically lie close to the disk, where $g(X) \simeq X$. Using equation (22a), $(X_{\rm cr}/W'_{\rm cr})^{1/2} \sim (1-\alpha/\alpha)^{1/2} \sim 1$. Both disk cases give, therefore, essentially the same result. We conclude that v_ϕ-terms can be important everywhere between the disk photosphere and the critical point and, hence, may modify $\dot{M}$.

To find their effect on $\dot{M}$, we include v_ϕ-terms in the evaluation of the line force, equation (2), in an approximate manner. Only the disk regime is considered, in which case the radiation intensity is roughly isotropic and the radiation flux has a z-component only. The azimuthal part of the solid angle integral in equation (2) is approximated by a four-point quadrature at angles $n\pi/2$ with $\hat{\boldsymbol{r}}$, where $n = 0, 1, 2, 3$. This leads to a correction factor of the approximate form $1/4(2 + |1+S|^\alpha + |1-S|^\alpha)$ to the line force, EfW'^α. Here, S is a linear combination of the expressions in equation (A1), with coefficients <1 from angle integration. In the disk regime, $S_{\rm cr} \sim 1$ from equation (A1). This coincides with the borderline between an increase and a decrease in $\dot{M}$ due to the inclusion of v_ϕ-terms, which lies at $S_{\rm cr} = 1.25$ for $\alpha = \frac{1}{2}$ and at $S_{\rm cr} = 1.18$ for $\alpha = \frac{2}{3}$. Hence, a detailed, numerical calculation of the above angle integral is required to decide which of both cases actually occurs. Since $S_{\rm cr}$ is close to unity, the influence on the mass-loss rate is limited to a 30% effect. We, therefore, neglect v_ϕ-terms in calculating the line force.

APPENDIX B

DISK WIND DECELERATION

In Figure 6, isocontours that cross through the low saddle point *loop* into one another at some larger height, X_d. At $X > X_d$, one has $E > E_{\rm cr}$ from the figure, i.e., the allowed maximum mass-loss rate in this region is *smaller* than that at the saddle. At these distances, inertia and gravity overcome the line force plus centrifugal force, and the wind decelerates, $W' < 0$. As is shown in Paper II, the wind speed always exceeds the *local* escape speed at X_d, which implies that the decelerating wind reaches infinity at a positive speed.

Because of the deceleration, the velocity law becomes nonmonotonic, and the line transfer is no longer purely local, because global couplings occur between distant resonance locations. We neglect these couplings and simply replace W'^α in the line force by $|W'|^\alpha$. For a wind ray launched at $r_0 = 5r_{\rm wd}$, Figure 8 shows that a single, decelerating branch, $W'_- < 0$, accompanies the critical, accelerating solution W'_+ of maximum mass-loss rate. It is suggestive that at X_d the solution curve jumps from the W'_+ to the W'_- branch and extends thereupon to infinity.

The discontinuity in W' introduces a *kink* in the velocity law. Such kinks propagate at sound speed (Courant & Friedrichs 1948; actually, for LDWs, at some modified, radiative-acoustic speed—see Abbott 1980 and Cranmer & Owocki 1996) and are therefore inconsistent with the assumption of stationarity. It seems plausible, however, that the discontinuity in W' is an artifact of the Sobolev approximation, since the latter becomes invalid at small dv_x/dx, i.e., as $W' \to 0$. An exact line transfer should instead give a smooth transition from W'_+ to W'_-. We find indeed cases of "almost" smooth transitions, where both $dW'_{+,-}/dX_d \to -\infty$, e.g., in the top panel of Figure 8.

REFERENCES

Abbott, D. C. 1980, ApJ, 242, 1183
———. 1982, ApJ, 259, 282
Arav, N., Shlosman, I., & Weymann, R. J., eds. 1997, ASP Conf. Ser. 128, Mass Ejection from Active Galactic Nuclei (San Francisco: ASP)
Begelman, M. C., McKee, C. F., & Shields, G. A. 1983, ApJ, 271, 70
Binney, J., & Tremaine, S. 1987, Galactic Dynamics (Princeton: Princeton Univ. Press)
Bjorkman, J. E. 1995, ApJ, 453, 369
Blandford, R. D., & Payne, D. G. 1982, MNRAS, 199, 883
Cannon, C. J., & Thomas, R. N. 1977, ApJ, 211, 910
Cassinelli, J. P. 1979, ARA&A, 17, 275
Castor, J. I. 1974, MNRAS, 169, 279
Castor, J. I., Abbott, D. C., & Klein, R. I. 1975, ApJ, 195, 157 (CAK)
Córdova, F. A., & Mason, K. O. 1982, ApJ, 260, 716
———. 1985, ApJ, 290, 671
Courant, R., & Friedrichs, K. O. 1948, Supersonic Flow and Shock Waves (New York: Interscience)
Cranmer, S. R., & Owocki, S. P. 1996, ApJ, 462, 469
Diaz, M. P., Wade, R. A., & Hubeny, I. 1996, ApJ, 459, 236
Emmering, R. T., Blandford, R. D., & Shlosman, I. 1992, ApJ, 385, 460
Feldmeier, A., Shlosman, I., & Vitello, P. 1999, ApJ, 526, 357 (Paper II)
Gayley, K. G., Owocki, S. P., & Cranmer, S. R. 1999, ApJ, 513, 442
Heap, S. R., et al. 1978, Nature, 275, 385
Holzer, T. E. 1977, J. Geophys. Res., 82, 23
Horne, K., & Cook, M. C. 1985, MNRAS, 214, 307
Horne, K., & Stiening, R. F. 1985, MNRAS, 216, 933
Icke, V. 1980, AJ, 85, 329
Klare, G., Wolf, B., Stahl, O., Krautter, J., Vogt, N., Wargau, W., & Rahe, J. 1982, A&A, 113, 76
Knigge, C., Woods, J. A., & Drew, J. E. 1995, MNRAS, 273, 225
Krautter, J., Vogt, N., Klare, G., Wolf, B., Duerbeck, H. W., Rahe, J., & Wargau, W. 1981, A&A, 102, 337
Kudritzki, R. P., Springmann, U., Puls, J., Pauldrach, A., & Lennon, M. 1998, in ASP Conf. Ser. 131, Boulder-Munich II: Properties of Hot, Luminous Stars, ed. I. Howarth (San Francisco: ASP), 278
Lamers, H., & Cassinelli, J. P. 1999, Introduction to Stellar Winds (Cambridge: Cambridge Univ. Press)
Livio, M. 1997, in ASP Conf. Ser. 121, Accretion Phenomena and Related Outflows, ed. D. T. Wickramasinghe, G. V. Bicknell, & L. Ferrario (San Francisco: ASP), 8
Lucy, L. B. 1975, Mem. Soc. R. Sci. Liège, 8, 359
Lucy, L. B., & Solomon, P. M. 1970, ApJ, 159, 879
Mauche, C. W., & Raymond, J. C. 1997, in Cosmic Winds and the Heliosphere, ed. J. R. Jokipii, C. P. Sonett, & M. S. Giampapa (Tucson: Univ. of Arizona Press), 111
Mauche, C. W., et al. 1999, in preparation
Mihalas, D., & Mihalas, B. 1984, Foundations of Radiation Hydrodynamics (New York: Oxford Univ. Press)
Owocki, S. P., Castor, J. I., & Rybicki, G. B. 1988, ApJ, 335, 914
Owocki, S. P., & Puls, J. 1996, ApJ, 462, 894
———. 1998, ApJ, 510, 355
Owocki, S. P., & Rybicki, G. B. 1984, ApJ, 284, 337
———. 1985, ApJ, 299, 265
———. 1986, ApJ, 309, 127
Pauldrach, A. 1987, A&A, 183, 295
Pauldrach, A., Kudritzki, R. P., Puls, J., Butler, K., & Hunsinger, J. 1994, A&A, 283, 525
Pauldrach, A., Puls, J., & Kudritzki, R. P. 1986, A&A, 164, 86
Pereyra, N. A., Kallman, T. R., & Blondin, J. M. 1997, ApJ, 477, 368
Poe, C. H., Owocki, S. P., & Castor, J. I. 1990, ApJ, 358, 199
Proga, D., Stone, J. M., & Drew, J. E. 1998, MNRAS, 295, 595 (PSD)
Pudritz, R. E., & Norman, C. A. 1986, ApJ, 301, 571
Puls, J., Springmann, U., & Lennon, M. 1999, in preparation
Puls, J., Springmann, U., & Owocki, S. P. 1998, in Cyclical Variability in Stellar Winds, ed. L. Kaper & A. W. Fullerton (Berlin: Springer), 389
Rutten, R. G., Dhillon, V. S., Horne, K., Kuulkers, E., & Van Paradijs, J. 1993, Nature, 362, 518
Shakura, N. I., & Sunyaev, R. A. 1973, A&A, 24, 337 (SHS)
Shlosman, I., & Vitello, P. 1993, ApJ, 409, 372
Shlosman, I., Vitello, P., & Mauche, C. W. 1996, ApJ, 461, 377
Shlosman, I., Vitello, P., & Shaviv, G. 1985, ApJ, 294, 96
Sobolev, V. V. 1957, Soviet Astron., 1, 678
Thomas, R. N. 1973, A&A, 29, 297
Vitello, P., & Shlosman, I. 1988, ApJ, 327, 680
———. 1993, ApJ, 410, 815
Woods, D. T., Klein, R. I., Castor, J. I., McKee, C. F., & Bell, J. B. 1996, ApJ, 461, 767